diameter and length of the nanotubes were obtained from about a hundred nanotubes in twenty transmission electron microscopy (TEM) images. The fNTs were characterized with a Jeol JEM-2010 TEM operating at 200 keV and a fluorescence spectrometer.

Loading Plasmid DNA into the Silica Nanotubes: The plasmid DNA encoding green fluorescence protein (GFP) (8 μg, Clontech) was added to the transparent nanotube (tNT) or fNT solution (200 μL) and mixed by rocking for 24 h at 4 °C. Unbound DNA was removed by washing with water several times. Finally, a $CaCl_2$ solution (2 μL, 2 M) was added to the DNA/nanotube complex solution, which was incubated for an additional 24 h. As a control, free DNA (8 μg) and tNTs without loaded DNA (200 μL) were treated independently with the $CaCl_2$ solution and incubated for 24 h under the same conditions as the DNA/nanotube complex.

GFP-Transfection Experiments: COS-7 cells were cultured in 10 cm dishes in Dulbecco's Modified Eagle Medium (DMEM) with 10 % fetal calf serum (FCS) in the presence of 1 % penicillin–streptomycin. The cells were grown at 37 °C in a CO_2 incubator and passaged every 2–3 days. For transfection experiments, the cells were seeded on 3 cm dishes for 24 h. The serum-containing DMEM was then removed from the dishes and replaced by 200 μL of the DNA/fNT complex. After 6 h, the residual DNA/fNT complex in the solution was removed by washing with phosphate-buffered saline (PBS) and replaced with fresh serum-containing DMEM. The cells were incubated continuously for 48 h. For contrast experiments, the cells were treated with free plasmid DNA or fNTs under the same conditions. For observation, the cells were washed with PBS and observed with an epifluorescence or laser-scanning confocal microscope. The number of cells was counted by flow cytometry (Partec).

3-(4,5-Dimethylthiazol-2-yl)-2,5-diphenyltetrazolium Bromide (MTT) Assay: Different amounts of fNTs (from 100–400 μL in 50 μL intervals) were added to COS-7 cells. After 48 h incubation, the MTT assay (Acros) was performed as described by the manufacturer. In brief, the serum-containing medium was replaced by the MTT solution (200 μL). After incubation in the MTT solution for 4 h, the cells were collected by centrifugation and treated with dimethyl sulfoxide (500 μL). The optical density at 570 nm was measured with a spectrometer (Bio-TEK).

Received: June 17, 2004
Final version: October 18, 2004
Published online: January 13, 2005

[1] a) C. R. Martin, P. Kohli, *Nat. Rev. Drug Discovery* **2003**, *2*, 29. b) A. P. Alivisatos, *Nat. Biotechnol.* **2004**, *22*, 47. c) C. M. Niemeyer, *Angew. Chem. Int. Ed.* **2001**, *40*, 4128.

[2] a) M. Bruchez, M. Moronne, P. Gin, S. Weiss, A. P. Alivisatos, *Science* **1998**, *281*, 2013. b) W. C. Chan, S. Nie, *Science* **1998**, *281*, 2016. c) C.-C. Lin, Y.-C. Yeh, C.-Y. Yang, C.-L. Chen, G.-F. Chen, C.-C. Chen, Y.-C. Wu, *J. Am. Chem. Soc.* **2002**, *124*, 3508.

[3] a) Y. Cui, Q. Q. Wei, H. K. Park, C. M. Lieber, *Science* **2001**, *293*, 1289. b) T. A. Taton, G. Lu, C. A. Mirkin, *J. Am. Chem. Soc.* **2001**, *123*, 5164. c) M. Shim, N. W. S. Kam, R. J. Chen, Y. M. Li, H. J. Dai, *Nano Lett.* **2002**, *2*, 285.

[4] D. T. Mitchell, S. B. Lee, L. Trofin, N. Li, T. K. Nevanen, H. Soderlund, C. R. Martin, *J. Am. Chem. Soc.* **2002**, *124*, 11 864.

[5] a) N. W. S. Kam, T. C. Jessop, P. A. Wender, H. Dai, *J. Am. Chem. Soc.* **2004**, *126*, 6850. b) M. Thomas, A. M. Klibanov, *Proc. Natl. Acad. Sci. U. S. A.* **2003**, *100*, 9138. c) T. Yamada, Y. Iwasaki, H. Tada, H. Iwabuki, M. K. L. Chuah, T. VandenDriessche, H. Fukuda, A. Kondo, M. Ueda, M. Seno, K. Tanizawa, S. Kuroda, *Nat. Biotechnol.* **2003**, *21*, 885. d) A. K. Salem, P. C. Searson, K. W. Leong, *Nat. Mater.* **2003**, *2*, 668. e) D. Pantarotto, J. P. Briand, M. Prato, A. Bianco, *Chem. Commun.* **2004**, 16.

[6] S. B. Lee, D. T. Mitchell, L. Trofin, T. K. Nevanen, H. Soderlund, C. R. Martin, *Science* **2002**, *296*, 2198.

[7] M. Zhang, Y. Bando, K. Wada, *J. Mater. Res.* **2000**, *15*, 387.

[8] a) E. D. Steinle, D. T. Mitchell, M. Wirtz, S. B. Lee, V. Y. Young, C. R. Martin, *Anal. Chem.* **2002**, *74*, 2416. b) R. G. Freeman, K. C. Grabar, K. J. Allison, R. M. Bright, J. A. Davis, A. P. Guthrie, M. B. Hommer, M. A. Jackson, P. C. Smith, D. G. Walter, M. J. Natan, *Science* **1995**, *267*, 1629.

[9] a) B. O. Dabbousi, J. Rodriguez-Viejo, F. V. Mikulec, J. R. Heine, H. Mattoussi, R. Ober, K. F. Jensen, M. G. Bawendi, *J. Phys. Chem. B* **1997**, *101*, 9463. b) X. G. Peng, T. E. Wilson, A. P. Alivisatos, P. G. Schultz, *Angew. Chem. Int. Ed. Engl.* **1997**, *36*, 145.

[10] I. M. Verma, N. Somia, *Nature* **1997**, *389*, 239.

[11] D. Luo, W. M. Saltzman, *Nat. Biotechnol.* **2000**, *18*, 33.

Self-Assembly and Electronics of Dipolar Linear Acenes**

By *Qian Miao*, *Michael Lefenfeld*, *Thuc-Quyen Nguyen*, *Theo Siegrist*, *Christian Kloc*, and *Colin Nuckolls**

Detailed below is an exploratory study into the synthesis, self-assembly, and electronics of new linear acenes (Fig. 1, compounds **1** and **2**) that are end-functionalized with a 1,4-quinone moiety. These molecules are unique because they have a static dipole moment incorporated into the well-known organic semiconductor skeleton of pentacene. Organic transistors[1,2] are projected to be an integral portion of new lightweight, flexible, and inexpensive plastic electronics.[3] Here we show the utility of donor–acceptor-mediated self-assembly in thin-film transistors and emphasize how important it is to control the balance between the molecule–molecule and molecule–substrate interactions. The created acenes (Fig. 1a) form antiparallel co-facial stacks with aromatic planes closer than the π–π distance in graphite by approximately 0.1 Å. In thin films, atomic force microscopy (AFM) shows that the molecules assemble into lamellae with the molecular long axis upright. Tailoring the self-assembly of these lamellae on the gate-dielectric surface[4,5] provides long-lived devices for this

[*] Prof. C. Nuckolls, Q. Miao, M. Lefenfeld, Dr. T.-Q. Nguyen
Department of Chemistry and The Nanoscience Center
Columbia University
New York, NY 10027 (USA)
E-mail: cn37@columbia.edu
Dr. T. Siegrist, Dr. C. Kloc
Bell Laboratories, Lucent Technologies
600 Mountain Ave., Murray Hill, NJ 07974 (USA)

[**] We thank Dr. Jochen Ulrich (Columbia) and Dr. David Lang (Lucent) for help in measuring the capacitance of the dielectric layers, and Dr. Michael Steigerwald (Columbia) for helpful discussions. We acknowledge primary financial support from the Nanoscale Science and Engineering Initiative of the National Science Foundation under NSF Award Number CHE-0117752 and by the New York State Office of Science, Technology, and Academic Research (NYSTAR) and the Department of Energy Nanoscience Initiative (NSET #04ER46118). C. N. acknowledges support from a Sloan Fellowship (2004), Camille Dreyfus Teacher–Scholar (2004), Beckman Young Investigator Program (2002), and the Dupont Young Investigator Program (2002). Supporting Information is available online from Wiley InterScience or from the author.

DOI: 10.1002/adma.200401251

ADVANCED MATERIALS

new class of dipolar organic semiconductors with useful field-effect mobilities ($>5\times10^{-2}$ cm^2 V^{-1} s^{-1} for **1**) and high ON/OFF-current ratios ($\geq10^6$).

Even though pentacene is one of the most electrically well-characterized of all organic-semiconductor materials, the number of linear-acene derivatives that have been synthesized and tested in transistors is small.[2] No derivatives of the longer acenes (e.g., hexacene) have been tested in organic field- effect transistor (OFET) applications. Remarkably, the hexacene quinone **1** can be quite easily synthesized in two steps from commercially available materials as shown in Scheme 1.[6] The first step utilizes a reaction found by Lepage and co-workers, where 2,5-dimethoxytetrahydrofuran is condensed with 1,2-benzene dialdehyde.[7] The stoichiometry controls whether naphthalene-, anthracene-, or tetracene-dialdehyde is produced. The previously unknown hexacene quinones can be conveniently synthesized by a second condensation of the tetracene dialdehyde with a 1,4-hydroquinone.[8] This method is general and has produced a number of hexacene and pentacene derivatives, such as the pentacene quinone **2** and the internal-hexacene quinone **3** (Fig. 1a).

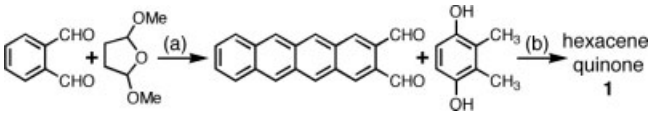

Scheme 1. Synthesis of **1**. a) Acetic acid, H2O, piperidine, reflux [7]. b) *p*-Toluenesulfonic acid, reflux.

Devices were fabricated[9] by first growing films using vacuum sublimation onto a silicon wafer, and then depositing gold source and drain electrodes through a metal mask. The device output is shown in Figure 2 for **1**. Compounds **2** and **3** are also p-type, hole-transporting semiconductors.[9,10] Given the strong electron-withdrawing nature of the quinone, it is remarkable that these materials are able to function as hole-transporting materials. The devices showed good stability and showed no apparent degradation in performance when tested periodically over the course of a few days.

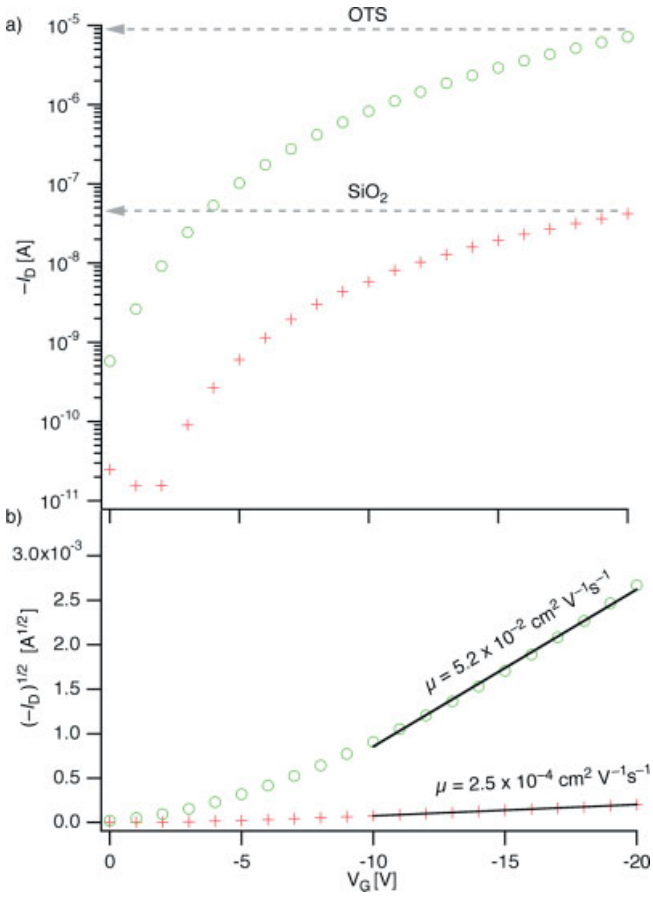

Figure 2. Transistor output for a top-contact device [10]. The channel length (L) and width (W) are 50 μm and 2 mm, respectively. The red crosses correspond to the device on SiO_2, and the green circles correspond to an OTS-coated SiO_2 dielectric layer. a) Plots of the source–drain current (I_D) versus the gate voltage V_G at a fixed drain voltage (–20 V). The ordinate is a logarithmic scale. b) Plots of the square root of the drain current versus the gate voltage at a fixed drain voltage (–20 V).

As shown in the current–voltage curves in Figure 2, there is a significant difference in the devices with the two dielectric surfaces. When the devices had clean but unfunctionalized SiO_2 as the dielectric layer (Fig. 2), the device characteristics

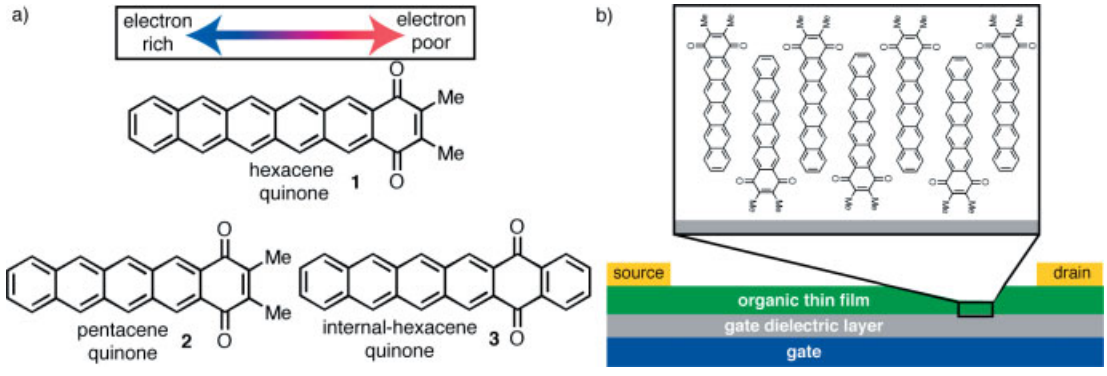

Figure 1. a) Structure of 2,3-dimethyl-1,4-hexacene-quinone (**1**), 2,3-dimethyl-1,4-pentacene-quinone (**2**), and 5,16-hexacene-quinone (**3**). b) Thin-film transistor structure highlighting the head-to-tail organization of **1**.

were poor. When a hydrophobic octadecyltrichlorosilane (OTS) monolayer[9,11] was installed on the silicon oxide, the source–drain current was over 200-times greater. While both pentacene and tetracene show some enhancements on silanized silicon oxide, the amounts that they increased were modest, with less than ten-times improvement.[12] We hypothesize that such a huge effect is seen for **1** due to the quinones being highly polar relative to the molecules traditionally[1–4] used in OFETs. (Other polar organic semiconductors can be found in the literature.[1g,1j,13])

Therefore, these molecules assemble very poorly on a polar gate-dielectric surface like SiO_2. Although the overall current levels for **2** and **3**[6] were lower, they also had enhancements on the OTS-treated silicon oxide.[10]

In order to compare the effective field-effect mobilities for the assemblies of **1** on the two different gate-dielectric materials, the capacitance of the dielectric films was measured[14] and found to be essentially the same for both the bare 100 nm SiO_2 (33 nF cm^{-2}) and OTS substrates (30 nF cm^{-2}). These values are in good agreement with the calculated values for a 100 nm SiO_2 substrate (34.5 nF cm^{-2}).[14] From the saturation regime of the data in Figure 2b and the capacitance measured above, the lower limit[15] on the saturation field-effect mobility for **1** was found to be 5.2×10^{-2} cm^2 V^{-1} s^{-1} when OTS was used (see Appendix). The ratio of the "ON" and "OFF" current levels was high ($\geq 10^6$).[16] Considering that these are the initial experiments on this class of compounds and there was no special optimization of the evaporation procedure, device geometry, or purity, these values are good. When the silicon oxide dielectric layer is used, the mobility for **1** is 2.5×10^{-4} cm^2 V^{-1} s^{-1}, which is lower than the device with the OTS substrate by a factor of 200 (see Appendix).

To better understand the assembly of these quinones, crystals of **1**, **2**, and **3** were grown using physical vapor transport crystallization.[17] Crystals of **2** were suitable for single-crystal X-ray diffraction. The top and side views of the structure reveal a head-to-tail, co-facial stack, as shown in Figure 3.[18] Analysis of the structure shown in Figure 3a shows that the aromatic planes are very closely spaced (<3.25 Å). This is closer than the interplanar distance in graphite sheets (3.35 Å) and likely a reflection of electrostatic self-complementarity in the π-surface of **2**, where an electron-rich acene portion stacks over an electron-poor quinoid portion. This mode of association forms one-dimensional columns. This head-to-tail arrangement for terminal quinones likely will be mimicked in **1** because it is seen in other quinones[19] and consistent with the model of Hunter and Sanders.[20] The magenta arrows in Figure 3b highlight interactions between the stacks where the carbonyls on the quinone come in close contact (C–O distance of approximately 2.8 Å) with two hydrogens in neighboring columns. This interaction provides the registration between neighboring columns.

X-ray diffraction from films of **1** (approximately 100 nm thick) on either silicon oxide or OTS-treated silicon oxide showed a lone diffraction peak at ca. 18.7–19.0 Å and peaks derived from this main peak up to the sixth order. This spacing is longer than the calculated length of **1**, but is similar to the expected length from models (approximately 19.0 Å) when it is stacked head-to-tail as in Figure 1b.[21] This indicates that the molecules in these films are organized in layers, with the long axis of the molecule being upright and the direction of π-stacking being parallel to the surface. Head-to-tail upright stacking is also supported by the morphology seen in the AFM images and the synchrotron X-ray reflectivity experiments outlined below.

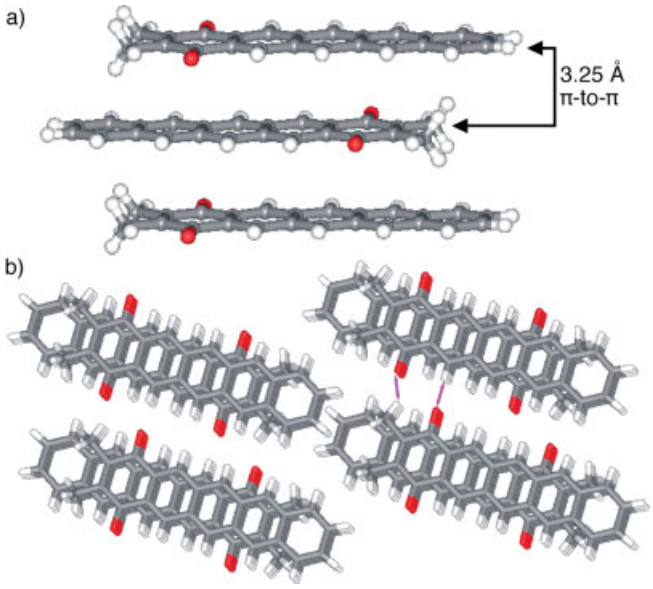

Figure 3. Views of the columnar crystal structure: a) side view, showing the π-stacking; b) top view, looking down the columnar axis; the magenta arrows show close contacts between columns.

Support for this π-stacked arrangement can be seen in the UV–vis spectra of **1** and **2,** shown in Figure 4. The longest wavelength transition in the UV–vis spectrum for **2** occurs at approximately 509 nm for the dimethyl pentacene quinone **2** in tetrahydrofuran (THF) solution (Fig. 4). This absorbance is red-shifted in films to 551 nm. Although **1** is not soluble enough to provide a UV–vis spectrum in solution, its films also exhibited shifted absorbances (at 680 nm) compared to the

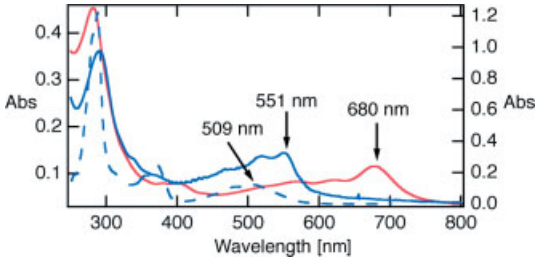

Figure 4. UV–vis spectrum of **1** and **2**. Left axis is for the UV–vis absorbance from films (approx. 40 nm thick on quartz) for **1** (red trace) and **2** (blue trace). The right axis is for the absorbance from THF solution (concentration $c = 3.9 \times 10^{-5}$ M, path length $L = 1$ cm) for **2** (dashed blue trace).

ADVANCED MATERIALS

calculated values for the long-wavelength absorbance maxima of 1,4-hexacene quinone.[13] These red-shifted absorbances result from delocalization of the excited state due to π-stacking.

To further investigate the self-organization of **1** on the OTS gate-dielectric surface, AFM measurements were made on films of varying thickness from sub-monolayer coverage to ca. 40 nm in thickness on OTS-treated silicon oxide.[9] AFM images of the thicker films (approximately 40 nm) of **1** show a layer-by-layer organization that produces terraced grains, shown in the representative micrograph in Figure 5a. The height of the lamellae are approximately 2.2 nm, similar to the lamellar spacing inferred from the thin-film X-ray diffraction experiments outlined above.

For thin films on OTS intended to be around one monolayer in height, the morphology shows a nearly complete initial layer of acenes covering the surface (Fig. 5b). Just as with the thicker films, the height of the layers is approximately 2.2 nm, indicating that the molecular long axis is upright in these initial layers. The monolayers form an interconnected network with no obvious crystalline facets. This morphology is distinct from the dendritic structures seen for linear acenes grown in thin films. (Pentacene and other acenes form a two-dimensional dendritic structure where the molecules are upright in the layer.[4])

After the first monolayer is deposited, the material continues to grow additional lamellae. Bilayer and trilayer regions are beginning to form in the image shown in Figure 5b.

To compare the morphology for films of **1** grown on SiO_2 and OTS-coated SiO_2, films of varying thickness were grown side-by-side in the same evaporation experiment.[9,11] For the thick films, the morphology shown in Figure 5a was essentially indistinguishable no matter which substrate was used. For the thin films of **1** shown in Figures 6a,b, again formed side-by-side, the morphology is very different. On bare silicon oxide, compound **1** forms small granular objects, while on OTS compound **1** forms the interconnected layers described above.

Synchrotron X-ray reflectivity measurements for thin films on either SiO_2 or OTS-coated SiO_2 qualitatively showed the same features as the AFM experiments. For monolayer coverage on silicon oxide, the films showed several relatively broad Bragg reflections indicating that the film was multiphasic. On the hydrophobic OTS surface, there was a singular and relatively sharp Bragg reflection at 2.0 nm. As the films were made thicker, up to about 7 nm, the position of this reflection on the OTS-coated surface remained constant. The implication is that the organization of the semiconductor at the gate-dielectric interface, when OTS is used, is similar to the bulk organization. Moreover, the Bragg spacing is longer than the calculated molecular length but consistent with the π-stacked assembly revealed in the crystal structure and depicted in Figure 1b. These reflectivity data, along with the bulk X-ray diffraction, AFM, and UV–vis measurements presented above, support the π-stacked, head-to-tail configurations depicted in Figure 1b.

The differences in the interfacial organization on the different substrates may arise from both the silicon oxide substrate and the quinone being polar. This similarity of the polarities slows the rate of surface diffusion (i.e., lateral growth) relative to the rate of vertical growth, and thereby creates numerous nucleation sites, defects, and imperfections in the initial molecular layers on SiO_2. When the surface is capped with the non-polar OTS group, the first layer of **1** is able to diffuse, self-assemble, and organize into a well-connected, compact monolayer.

The experiments above put forth a new class of dipolar linear acenes that self-assemble to form close-packed, co-facially stacked columnar superstructures. The molecule is self-complementary, having electron-rich and electron-poor segments, and forms an antiparallel association in the solid state. The

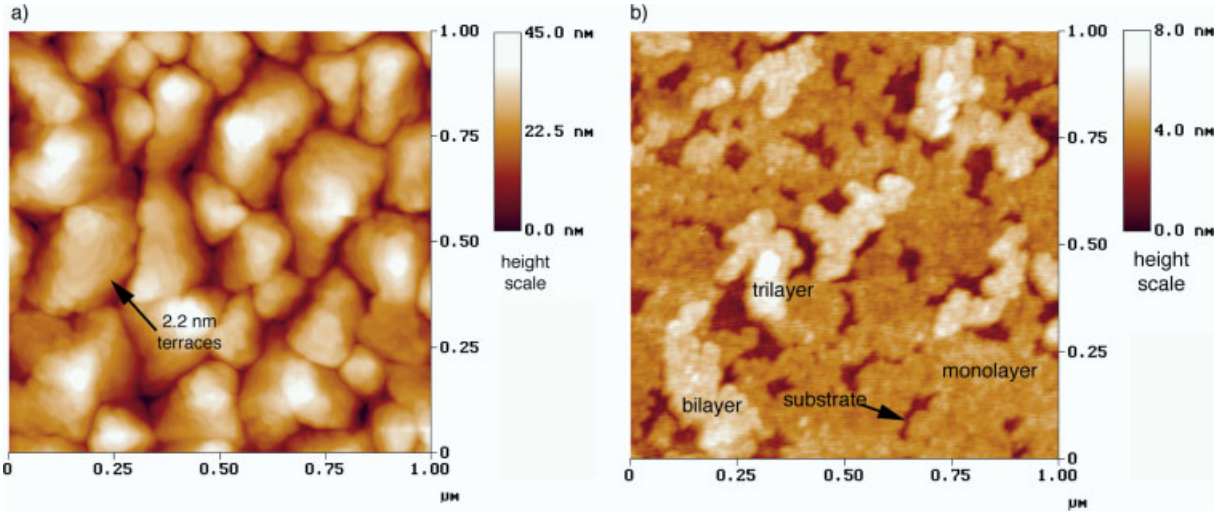

Figure 5. AFM images of thermally evaporated films on a substrate that was held at approx. 100 °C: a) 1 μm × 1 μm scan of **1** on OTS-treated silicon oxide with a roughly 40 nm thick film, showing molecular terraces. b) 1 μm × 1 μm AFM scan of **1** on OTS-treated silicon oxide showing monolayers, bilayers, and trilayers.

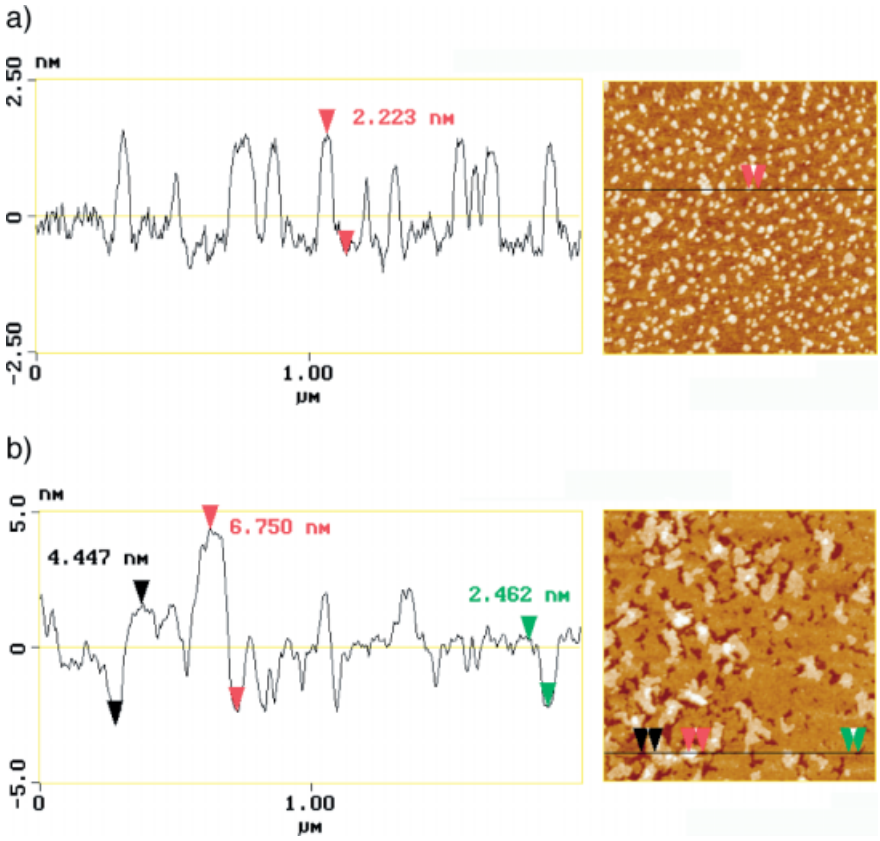

Figure 6. AFM cross-sectional height image (2 μm × 2 μm scan) of a) a bare SiO_2 substrate with a submonolayer of **1** and b) an OTS-treated SiO_2 substrate with a submonolayer of **1**.

field-effect mobilities and ON/OFF ratios are in a range that could be useful in plastic electronic devices. More broadly, these dipolar molecular semiconductors provide an untested route to "self-wiring" of organic electronic components by using electric fields to direct the assembly of electroactive molecules.

Experimental

Wafer Cleaning and Octadecyltrichlorosilane (OTS) Functionalization and Transistor Fabrication: Electrical measurements were performed on a highly n-type doped (< 0.005 Ω cm) Si wafer, used as a shared common gate, for the quinone semiconductor thin films. Top-contact geometry was used in the transistor devices. A 100 nm or 300 nm thick, thermally grown SiO_2 layer served as the gate dielectric. Two surface treatments of the SiO_2 were performed before vacuum sublimation of the semiconductor film: a) for bare SiO_2, exposure to an oxidative plasma, and b) for OTS-coated SiO_2, a 10 min sonication in acetone, followed by a 70:30 (vol./vol.) H_2SO_4/H_2O_2 (piranha) etch for 1 h at 100 °C, then a 1:1:5 $NH_3{\cdot}H_2O/H_2O_2$/deionized water wash for 20 min at 70 °C, and finally a soak in a 25 mM solution of OTS in toluene at 28 °C for 1 h. The dielectric surface was characterized using water-contact-angle measurements, which were < 5° after cleaning and > 105° after OTS-monolayer formation. The semiconductor thin films were vacuum-deposited by an Edwards Auto 306 vacuum coater with the turbomolecular pump set to a pressure of 2.0×10^{-4} Pa or lower, with a deposition rate of ca. 1 Å s^{-1} to the desired thickness. Different substrate temperatures for deposition were achieved using a radiant heater with a reflector, with the temperature being measured with a thermocouple. The drain and source electrodes were vacuum-deposited through a shadow mask, and the resulting semiconducting channels were 50 μm long and 2 mm wide. Thin-film transistor characterization was carried out at room temperature in ambient atmosphere using a Keithley 4200-SCS semiconductor parameter analyzer.

Atomic Force Microscopy (AFM) Measurements: Topographic images were obtained using a Nanoscope IIIa/Bioscope Scanning Probe Microscope from Digital Instruments. Etched silicon tips with a typical spring constant of 1–5 N m^{-1} and a resonant frequency of 50–80 kHz (NanoSensors) were used. All AFM images were collected using tapping mode and in air under ambient conditions. The topographic images were collected from multiple samples, and for each sample, ten or more regions were scanned to ensure reproducibility.

Appendix

The mobility was calculated [1a] in the saturation region of the *I–V* curves in Figure 2b using

$$I_D = (WC_i/2L)[\mu_{fet}(V_G - V_T)^2] \quad (1)$$

where I_D is the source–drain current, μ_{fet} is the field-effect mobility, V_G is the gate voltage, and V_T is the threshold voltage. The channel length (L) and width (W) are 50 μm and 2 mm, respectively. The capacitances of the gate dielectric layer (C_i) are 11.3 nF cm^{-2} and 30 nF cm^{-2} for 300 nm and 100 nm thick OTS-treated silicon oxide layers, respectively, while the capacitances are 11.5 nF cm^{-2} and 33 nF cm^{-2} for 300 nm thick and 100 nm thick silicon oxide layers, respectively.

Received: August 2, 2004
Final version: September 8, 2004
Published online: January 18, 2005

ADVANCED MATERIALS

[1] a) C. D. Dimitrakopoulos, P. R. L. Malenfant, *Adv. Mater.* **2002**, *14*, 99. b) Y.-Y. Lin, D. J. Gundlach, S. F. Nelson, T. N. Jackson, *IEEE Trans. Electron Devices* **1997**, *44*, 1325. c) D. J. Gundlach, Y. Y. Lin, T. N. Jackson, D. G. Schlom, *Appl. Phys. Lett.* **1997**, *71*, 3853. d) F. Garnier, *Chem. Phys.* **1998**, *227*, 253. e) Z. Bao, A. J. Lovinger, J. Brown, *J. Am. Chem. Soc.* **1998**, *120*, 207. f) G. Horowitz, *J. Mater. Chem.* **1999**, *9*, 2021. g) H. E. Katz, A. J. Lovinger, J. Johnson, C. Kloc, T. Siegrist, W. Li, Y. Y. Lin, A. Dodabalapur, *Nature* **2000**, *404*, 478. h) H. E. Katz, Z. Bao, S. L. Gilat, *Acc. Chem. Res.* **2001**, *34*, 359. i) D. J. Gundlach, J. A. Nichols, L. Zhou, T. N. Jackson, *Appl. Phys. Lett.* **2002**, *80*, 2925. j) T. M. Pappenfus, R. J. Chesterfield, C. D. Frisbie, K. R. Mann, J. Casado, J. D. Raff, L. L. Miller, *J. Am. Chem. Soc.* **2002**, *124*, 4184. k) M. Mushrush, A. Facchetti, M. Lefenfeld, H. E. Katz, T. J. Marks, *J. Am. Chem. Soc.* **2003**, *125*, 9414. l) K. Ito, T. Suzuki, Y. Sakamoto, D. Kubota, Y. Inoue, F. Sato, S. Tokito, *Angew. Chem. Int. Ed.* **2003**, *42*, 1159. m) Q. Miao, T.-Q. Nguyen, T. Someya, G. B. Blanchet, C. Nuckolls, *J. Am. Chem. Soc.* **2003**, *125*, 10 284. n) H. E. Katz, J. Otsuki, K. Yamazaki, A. Suka, T. Takido, A. J. Lovinger, K. Raghavachari, *Chem. Lett.* **2003**, *32*, 508.

[2] a) C. D. Sheraw, T. N. Jackson, D. L. Eaton, J. E. Anthony, *Adv. Mater.* **2003**, *15*, 2009. b) H. Meng, M. Bendikov, G. Mitchell, R. Helgeson, F. Wudl, Z. Bao, T. Siegrist, C. Kloc, C.-H. Chen, *Adv. Mater.* **2003**, *15*, 1090.

[3] a) D. Voss, *Nature* **2000**, *407*, 442. b) C. J. Drury, C. M. J. Mutsaers, C. M. Hart, M. Matters, D. M. de Leeuw, *Appl. Phys. Lett.* **1998**, *73*, 108. c) J. A. Rogers, Z. Bao, K. Baldwin, A. Dodabalapur, B. Crone, V. R. Raju, V. Kuck, H. Katz, K. Amundson, J. Ewing, P. Drzaic, *Proc. Natl. Acad. Sci. U. S. A.* **2001**, *98*, 4835. d) J. A. Rogers, Z. Bao, *J. Polym. Sci., Part A: Polym. Chem.* **2002**, *40*, 3327. e) Y.-L. Loo, T. Someya, K. W. Baldwin, Z. Bao, P. Ho, A. Dodabalapur, H. E. Katz, J. A. Rogers, *Proc. Natl. Acad. Sci. U. S. A.* **2002**, *99*, 10 252. f) G. B. Blanchet, Y.-L. Loo, J. A. Rogers, F. Gao, C. R. Fincher, *Appl. Phys. Lett.* **2003**, *82*, 463. g) G. H. Gelinck, H. E. A. Huitema, E. van Veenendaal, E. Cantatore, L. Schrijnemakers, J. B. P. H. van der Putten, T. C. T. Geuns, M. Beenhakkers, J. B. Giesbers, B.-H. Huisman, E. J. Meijer, E. M. Benito, F. J. Touwslager, A. W. Marsman, B. J. E. van Rens, D. M. de Leeuw, *Nat. Mater.* **2004**, *3*, 106.

[4] a) G. Horowitz, X. Z. Peng, D. Fichou, F. Garnier, *Synth. Met.* **1992**, *51*, 419. b) F. J. Meyer zu Heringdorf, M. C. Reuter, R. M. Tromp, *Nature* **2001**, *412*, 517. c) K. P. Weidkamp, C. A. Hacker, M. P. Schwartz, X. Cao, R. M. Tromp, R. J. Hamers, *J. Phys. Chem. B* **2003**, *107*, 11 142. d) F. J. Meyer zu Heringdorf, M. C. Reuter, R. M. Tromp, *Appl. Phys. A: Mater. Sci. Process.* **2004**, *78*, 787. e) S. E. Fritz, S. M. Martin, C. D. Frisbie, M. D. Ward, M. F. Toney, *J. Am. Chem. Soc.* **2004**, *126*, 4084.

[5] A. Dodabalapur, L. Torsi, H. E. Katz, *Science* **1995**, *268*, 270.

[6] Synthetic details and characterization for compounds **1–3** can be found in the Supporting Information.

[7] A. Mallouli, Y. Lepage, *Synthesis* **1980**, *9*, 689.

[8] L. Lepage, Y. Lepage, *Synthesis* **1982**, *10*, 882.

[9] See the Experimental section for the details of the cleaning and functionalization of the silicon wafers, device fabrication, thermal evaporation of compounds **1–3**, and the AFM measurements.

[10] The data presented in Figure 2 was for a 100 °C substrate temperature during deposition. Results at other substrate temperatures for compounds **1–3** can be found in the Supporting Information.

[11] OTS functionalization of silicon oxide: a) I. Haller, *J. Am. Chem. Soc.* **1978**, *100*, 8050. b) J. Gun, R. Iscovici, J. Sagiv, *J. Colloid Interface Sci.* **1984**, *101*, 201. c) S. R. Wasserman, Y. T. Tao, G. M. Whitesides, *Langmuir* **1989**, *5*, 1074.

[12] In thin films, pentacene has field-effect mobilities as high as 0.7 $cm^2 V^{-1} s^{-1}$ on SiO_2 [1b]. Values for the field-effect mobility are about three to four times higher on hydrophilic surfaces; see a) S. F. Nelson, Y.-Y. Lin, D. J. Gundlach, T. N. Jackson, *Appl. Phys. Lett.* **1998**, *72*, 1854. b) T. W. Kelley, L. D. Boardman, T. D. Dunbar, D. V. Muyres, M. J. Pellerite, T. P. Smith, *J. Phys. Chem. B* **2003**, *107*, 5877. c) H. Klauk, M. Halik, U. Zschieschang, G. Schmid, W. Radlik, W. Weber, *J. Appl. Phys.* **2002**, *92*, 5259. d) M. Shtein, J. Mapel, J. B. Benziger, S. R. Forrest, *Appl. Phys. Lett.* **2002**, *81*, 268. Similar to pentacene, tetracene shows a modest enhancement when OTS-coated silicon oxide is used [1c].

[13] K. Hiruta, S. Tokita, K. Nishimoto, *Dyes Pigm.* **1998**, *38*, 165.

[14] The measured capacitance was essentially the same for both the OTS-treated silicon oxide (300 nm: 11.3 nF cm^{-2}; 100 nm: 30 nF cm^{-2}) and for the silicon oxide (300 nm: 11.5 nF cm^{-2}; 100 nm: 33 nF cm^{-2}). The capacitance measurements were invariant over a range of frequencies (100 Hz to 1 MHz) and showed little change with and without illumination. The values used in the literature for OTS-coated silicon oxide vary over a wide range (compare the values in [1i] and [12d]). The calculated capacitance per unit area for an idealized 100 nm thick silicon oxide layer is 34.52 nF cm^{-2}; see S. M. Sze, *Physics of Semiconductor Devices*, 1st ed, Wiley, New York **1969**.

[15] The intrinsic mobility of the material must be higher because the calculation of the mobility assumes that all of the charge in the capacitor is converted into mobile carriers; see V. Y. Butko, X. Chi, D. V. Lang, A. P. Ramirez, *Appl. Phys. Lett.* **2003**, *83*, 4773.

[16] This is the ratio of the drain current for a device with a 300 nm SiO_2 dielectric layer coated with OTS at gate voltages (V_G) of $V_G = 0$ V (OFF) and $V_G = -100$ V (ON).

[17] R. A. Laudise, C. Kloc, P. G. Simpkins, T. Siegrist, *J. Cryst. Growth* **1998**, *187*, 449.

[18] The crystallographic information file (.cif) is contained in the Supporting Information.

[19] a) A. V. Dzyabchenko, V. E. Zavodnik, V. K. Bel'skii, *Acta Crystallogr., Sect. B: Struct. Crystallogr. Cryst. Chem.* **1979**, *B35*, 2250. b) A. V. Dzyabchenko, V. E. Zavodnik, *Zh. Strukt. Khim.* **1984**, *25*, 177.

[20] C. A. Hunter, J. K. M. Sanders, *J. Am. Chem. Soc.* **1990**, *112*, 5525.

[21] This type of arrangement has been seen for some π-stacked n-type materials: R. J. Chesterfield, C. R. Newman, T. M. Pappenfus, P. C. Ewbank, M. H. Haukaas, K. R. Mann, L. L. Miller, C. D. Frisbie, *Adv. Mater.* **2003**, *15*, 1278.

Rapid Thermal Synthesis of Silver Nanoprisms with Chemically Tailorable Thickness**

By *Gabriella S. Métraux* and *Chad A. Mirkin**

Several methods have been developed for synthesizing Ag and Au nanoparticles in a variety of shapes, including disks,[1–4] rods,[5–9] prisms,[10–14] wires,[15–18] hollow structures,[19–22] and branched particles.[23] Recently, there has been

[*] Prof. C. A. Mirkin, G. S. Métraux
Department of Chemistry and Institute for Nanotechnology
Northwestern University
2145 Sheridan Road, Evanston, IL 60208 (USA)
E-mail: chadnano@northwestern.edu

[**] We would like to thank E. C. Hao and Prof. G. C. Schatz for the DDA calculations presented in this paper. The ONR and NSF-NSEC program have supported this work. Supporting Information is available online from Wiley InterScience or from the author.

  DOI: 10.1002/adma.200401086